ECCOMAS Congress 2016
VII European Congress on Computational Methods in Applied Sciences and Engineering
M. Papadrakakis, V. Papadopoulos, G. Stefanou, V. Plevris (eds.)
Crete Island, Greece, 5–10 June 2016

BS1 - DNS OF THE TAYLOR-GREEN VORTEX AT RE $= 1600$

A. Mastellone[1], L. Cutrone[1] and F. Capuano[2]

[1]Centro Italiano per le Ricerche Aerospaziali (CIRA)
Via Maiorise, I-81043 Capua (Italy)
e-mail: a.mastellone@cira.it

[2] Dipartimento di Ingegneria Industriale, Università di Napoli "Federico II"
Via Claudio 21 - I-80125 Napoli (Italy)
e-mail: francesco.capuano@unina.it

Keywords: LES. High-order schemes. Turbulence.

Abstract. *SPARK-LES is a Large-Eddy Simulation (LES) code currently under development at the Italian Aerospace Reseacrh Center (CIRA). It solves the fully compressible Navier-Stokes equations discretized on multi-block, structured grids according to the Finite-Volume (FV) method, using different high-order schemes. In this work a detailed comparison between the schemes is presented in the simulation of a Taylor-Green Vortex in order to assess their accuracy and performances. Temporal behaviour of kinetic energy decay rate and enstrophy is given at different mesh resolutions, showing a good agreeement with DNS results at finer grids. Analysis of power spectra confirms the universal energy cascade behavior.*

1 Code description

SPARK-LES is a Large-Eddy Simulation (LES) code currently under development at CIRA in the framework of the HYPROB Program, funded by the Italian Ministry of Research [1]. The code shall be an advanced tool with high-fidelity numerical methods and state-of-the-art modelling, and able to reproduce the operation of a liquid-rocket thrust chamber at high pressures. This feature will support design of critical components of the chamber, like injectors, cooling channels, etc; and analysis of unsteady phenomena of combustion instabilities.

SPARK-LES solves the fully compressible Navier-Stokes equations discretized on multi-block, structured grids according to the Finite-Volume (FV) method. Explicit second- and fourth-order (2E, 4E), as well as fourth- and sixth-order compact (4C, 6C) cartesian-like operators are available for reconstruction of convective fluxes, whereas an explicit second-order scheme is used for diffusive fluxes [2]. The general interpolation operator can be expressed, for a generic variable ϕ, as

$$\alpha\tilde{\phi}_{i-3/2} + \tilde{\phi}_{i-1/2} + \alpha\tilde{\phi}_{i+1/2} = \sum_{j=1}^{N_C} \gamma_j \left(\bar{\phi}_{i-j} + \bar{\phi}_{i+j-1}\right), \tag{1}$$

where $\tilde{\phi}$ and $\bar{\phi}$ are the face- and cell-averaged values of ϕ, respectively.

The tridiagonal system arising from Eq. (1) when $\alpha \neq 0$ is solved by means of a Thomas algorithm. In the case of a multi-block domain, an *overlap* method is adopted [3]: for each block, an enlarged linear system is solved by overlapping a certain number of neighbour cells from adjacent blocks (in this study 4 cells are used, which are a good tradeoff between parallel communication overhead and scheme accuracy). The boundary points at block-to-block interfaces are evaluated by a high-order centered approximation formula.

Time-advancement is obtained by means of explicit Runge-Kutta schemes of arbitrary number of stages. SPARK-LES features an MPI parallel implementation based on the multi-block partitioning of the computational domain. The MPI calls have been carefully profiled in order to minimize communication overhead. The code makes full use of Fortran 90 capabilities, in terms of dynamic allocation, highly modular architecture and massive use of pointers for CPU efficiency and memory usage optimization.

2 Case summary

The Taylor-Green Vortex problem is defined on a triperiodic cube with sides of 2π, $L = 1$ and the following initial conditions

$$u_x(x,y,z) = U_0 \sin(x/L)\cos(y/L)\cos(z/L), \tag{2}$$

$$u_y(x,y,z) = -U_0 \cos(x/L)\sin(y/L)\cos(z/L), \tag{3}$$

$$u_z(x,y,z) = 0, \tag{4}$$

$$p(x,y,z) = p_0 + \frac{\rho_0 U_0^2}{16}\left[\cos(2x/L) + \cos(2y/L)\right]\left[\cos(2z/L) + 2\right] \tag{5}$$

As time advances, the initial distribution of vorticity is subject to vortex-stretching, thus generating small scales and eventually causing the vortices to break into turbulence. Since there is no forcing to sustain the turbulent motion, a decay is observed after transition. The incompressible problem is entirely governed by the Reynolds number $Re = \frac{\rho U_0 L}{\mu}$, equal to 1600. However,

Figure 1: Kinetic energy dissipation rate as a function of the non-dimensional time t^* for second-order (left) and fourth-order (right) explicit schemes.

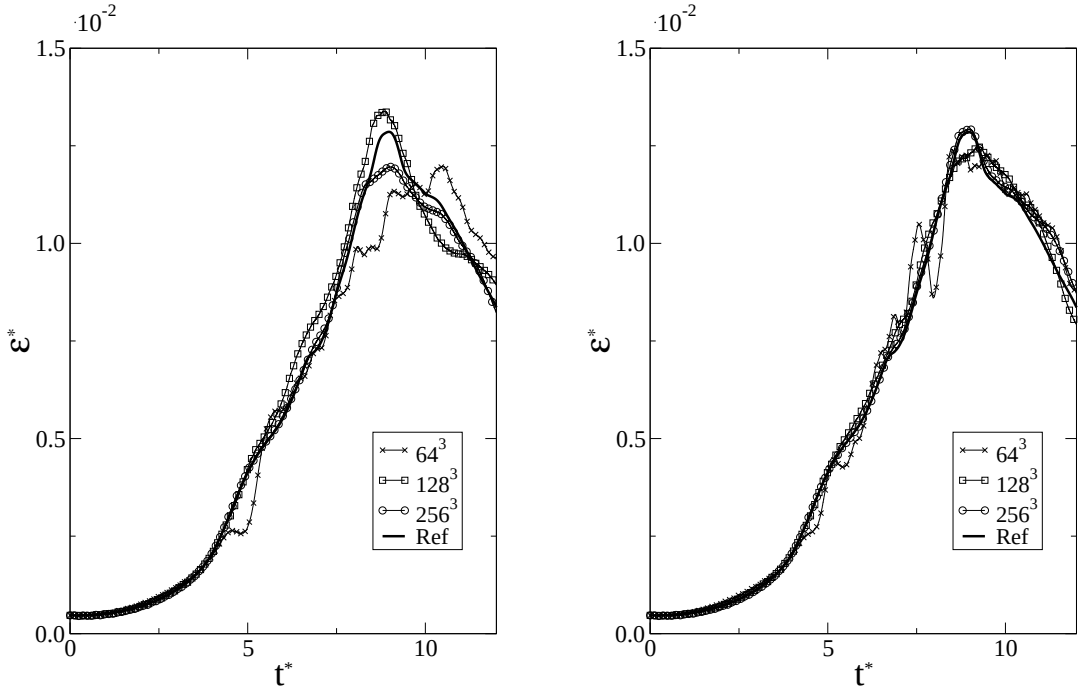

since the code solves the compressible flow equations, the other dimensional parameters have been set to yield a nearly incompressible condition, i.e. $M = 0.1$. The ideal gas equation of state is used, along with a constant Prandtl number $Pr = 0.71$. The domain has been discretized by a uniform mesh of increasing resolution, 64^3, 128^3 and 256^3 cells, divided in 64 equally-sized blocks. The meshes are regular cartesian grids and have been generated by an in-house tool. In this study, explicit second- and fourth-order and compact fourth- and sixth-order schemes are used. The coefficients of Eq. (1) are $\gamma_1 = 1/2$ for the explicit second-order scheme ($\alpha = 0$, $N_C = 1$), $\gamma_1 = 7/12$ and $\gamma_2 = -1/12$ for the explicit fourth-order scheme ($\alpha = 0$, $N_C = 2$), $\gamma_1 = 3/4$ for the fourth-order compact scheme ($\alpha = 1/4$, $N_C = 1$), and $\gamma_1 = 29/36$ and $\gamma_2 = 1/36$ for the sixth-order compact scheme ($\alpha = 1/3$, $N_C = 2$). Time-advancement is performed using a third-order Runge-Kutta scheme with CFL $= 0.6$. No artificial dissipation or filters of any type are used. The computations were run on the CIRA cluster FLAME, equipped with Intel Xeon E5-2680 @2.7 GHz processors. All simulations have been carried over 64 MPI nodes, assigning one block to each node. Results from TauBench runs gave an average time of 7.344 s.

3 Results

Figures 1 and 2 show the time-evolution of the global kinetic energy dissipation rate

$$\varepsilon = \frac{d}{dt}\frac{1}{\rho_0 \Omega}\int_\Omega \rho \frac{u_i u_i}{2} d\Omega \tag{6}$$

for different schemes and for three grid resolutions. The time t^* is adimensionalized by means of L and U_0. A good grid convergence is observed in all cases. The finest grid is in excellent agreement with the reference solution. The coarse grid shows an oscillatory behavior probably

Figure 2: Kinetic energy dissipation rate as a function of the non-dimensional time t^* for fourth-order (left) and sixth-order (right) compact schemes.

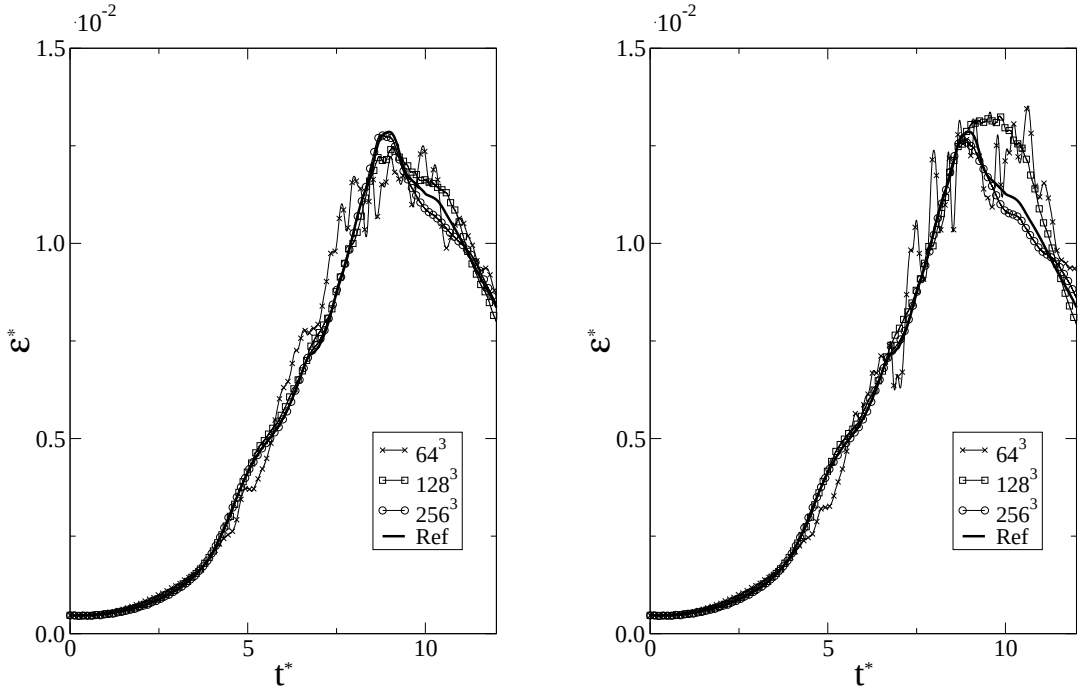

due to inadequate resolution as the flow undergoes creation of smaller scales. The integrated enstrophy

$$\zeta = \frac{1}{\rho_0 \Omega} \int_\Omega \rho \frac{\omega_i \omega_i}{2} d\Omega \tag{7}$$

is also considered: this is as an indirect measure of the dissipation rate, through the relation $\varepsilon_\zeta = 2\frac{\mu}{\rho_0}\zeta$. The time-evolution of ε_ζ is shown in Figs. 3 and 4. For the finest resolution, good agreement is observed also for the enstrophy-based dissipation rate, hence no significant spurious dissipation is added to the solution and turbulent scales are well resolved by the numerical scheme. At lower resolutions, the enstrophy-based dissipation rate is lower than the kinetic energy dissipation rate, suggesting that there are numerical dissipation sources [4].

Contours of the vorticity norm on a subset of the plane $x = -\pi L$ at $t^* = 8$ are shown in Figures 5 and 6. While the lowest grid resolution captures only the concentration of vorticity, the main structures of the shear layer are described increasingly well as the mesh is refined. The result on 256^3 cells shows a satisfactory agreement with the reference solution [5]. Although the presence of spurious secondary structures is still observed, the vorticity contours are well defined for high order (> 2) schemes, showing adequate resolution.

Kinetic energy spectra are defined as

$$P(k) = \frac{1}{2}\left(\tilde{u}_x \tilde{u}_x^* + \tilde{u}_y \tilde{u}_y^* + \tilde{u}_z \tilde{u}_z^*\right), \quad k = \sqrt{k_x^2 + k_y^2 + k_z^2} \tag{8}$$

being $\tilde{u}_i$ ($i \in \{x, y, z\}$) the 3D discrete Fourier transform of the i-th velocity component u_i.

$$\tilde{u}_i(k_x, k_y, k_z) = \frac{1}{N^3} \sum_{p=0}^{N-1} \sum_{q=0}^{N-1} \sum_{r=0}^{N-1} u_i(x_p, y_q, z_r) \cdot \exp\left(-ik_x x_p\right) \exp\left(-ik_y y_q\right) \exp\left(-ik_z z_r\right) \tag{9}$$

Figure 3: Enstrophy-based dissipation rate as a function of the non-dimensional time t^* for second-order (left) and fourth-order (right) explicit schemes.

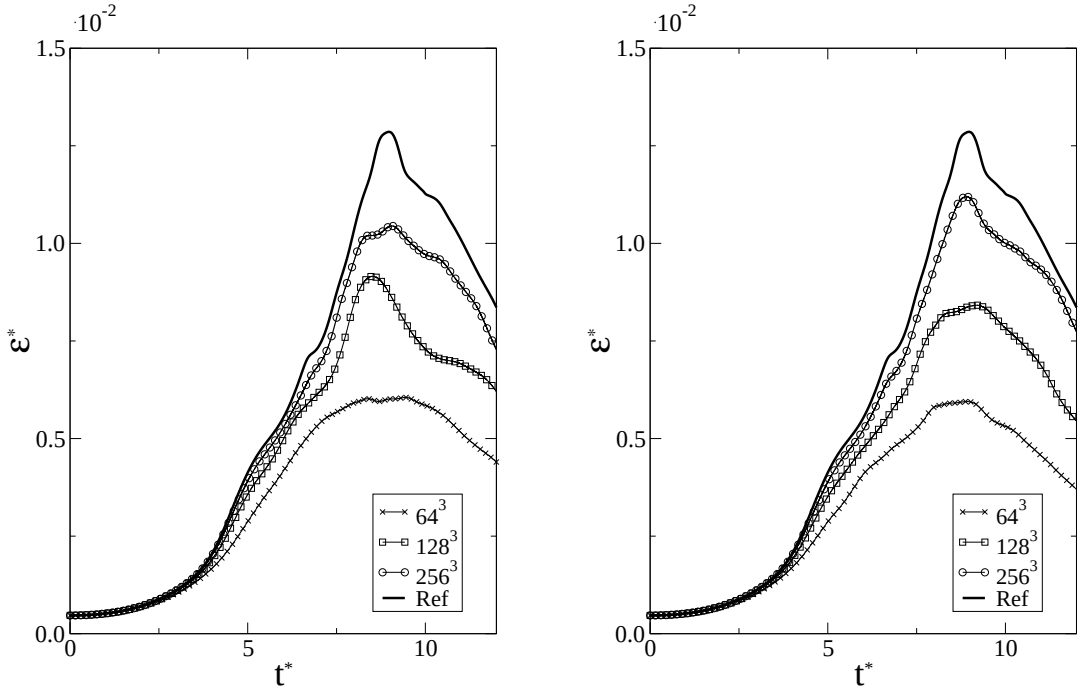

and the wavenumbers are limited by the condition $|k| < \pi N/L$, being N^3 the number of cells in the domain. They give a precise idea of the energy scale behavior. Figures 7 and 8 show that the spectra are substantially independent of the scheme giving the expected universal behavior at finer grids. The lowest resolution shows significant pile-up of energy at higher wavenumbers due to the accumulation of aliasing errors. The pile-up disappears as the number of mesh points is increased.

Simulation times are reported in Table 1. A decrease of performance is present in parallel runs due to the communication overhead, increasing with the number of layers used for different schemes (2E : one layer; 4E : two layers; 4C and 6C : four layers).

REFERENCES

[1] Borrelli, S., de Matteis, P., Schettino, A. and Ferrigno, F., "The HYPROB Program: mastering key technologies, design and testing capabilities for space transportation rocket propulsion evolution," *Proceedings of the 63th International Astronautical Congress*, Naples (2012), pp. 7189-7190.

[2] Fosso, P., A., Deniau, H., Sicot, F. and Sagaut, P., "Curvilinear finite-volume schemes using high-order compact interpolation," *J. Comput. Phys.* (2010), **229**:5090–5122.

[3] Capuano, F., and Mastellone, A., "Parallelization of compact finite-volume schemes for turbulent compressible flow", *Proceedings of 27th International Conference on Parallel Computational Fluid Dynamics (PARCFD 2015)*, Montreal (2015), in press.

[4] DeBonis, J. R., "Solutions of the Taylor-Green Vortex Problem Using High-Resolution Explicit Finite Difference Methods", NASA/TM2013-217850.

Figure 4: Enstrophy-based dissipation rate as a function of the non-dimensional time t^* for fourth-order (left) and sixth-order (right) compact schemes.

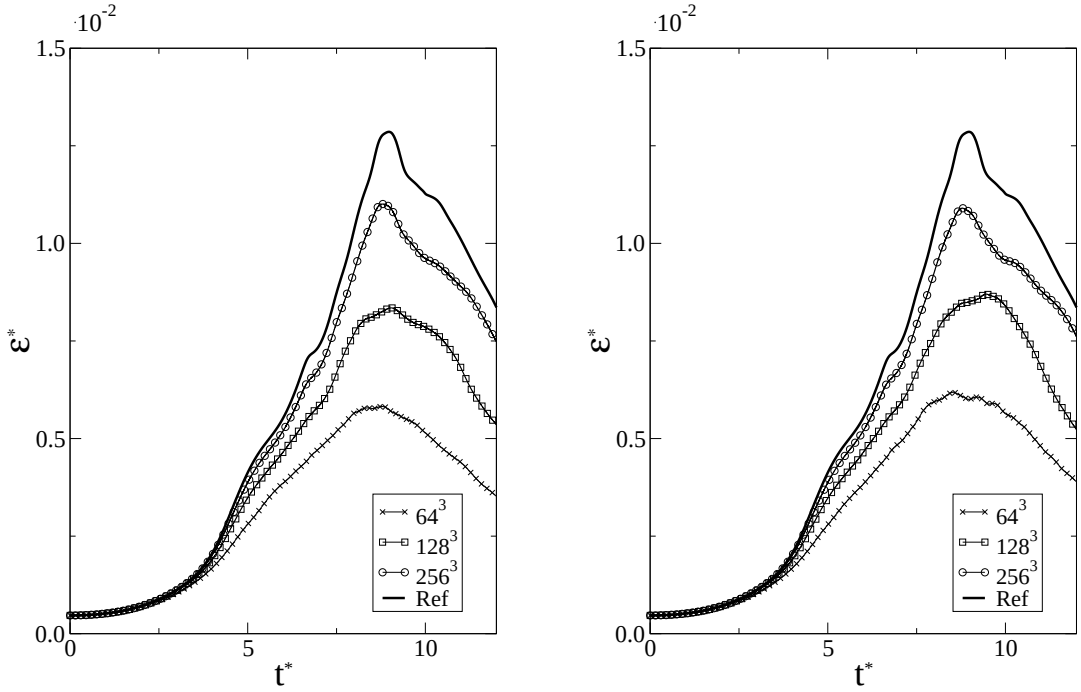

[5] van Rees, W.M., Leonard, A., Pullin, D.I. and Koumoutsakos, P., "A comparison of vortex and pseudo-spectral methods for the simulation of periodic vortical flows at high Reynolds numbers," *J. Comput. Phys.* (2011), **230**:2794–2805.

Table 1: TauBench-normalized costs to integrate until $t^* = 10$. MPI and serial refer to runs over 64 and single node. Serial runs have been verified to show about same execution time for all the schemes.

N	Scheme	Total Work Units	
		MPI	Serial
64	2E	1180	942
64	4E	1420	
64	4C	1626	
64	6C	1662	
128	2E	20945	15125
128	4E	23571	
128	4C	25633	
128	6C	25978	
256	2E	311457	243567
256	4E	352837	
256	4C	380245	
256	6C	382699	

Figure 5: Contour of dimensionless vorticity norm $\frac{L}{U_0}\|\omega\| = 1, 5, 10, 20, 30$ in a subset of the periodic face $\frac{x}{L} = -\pi$ at time $t^* = 8$ on the three grids. Comparison between reference results in [5] (red) and SPARK-LES results (black) for second-order (left) and fourth-order (right) explicit schemes.

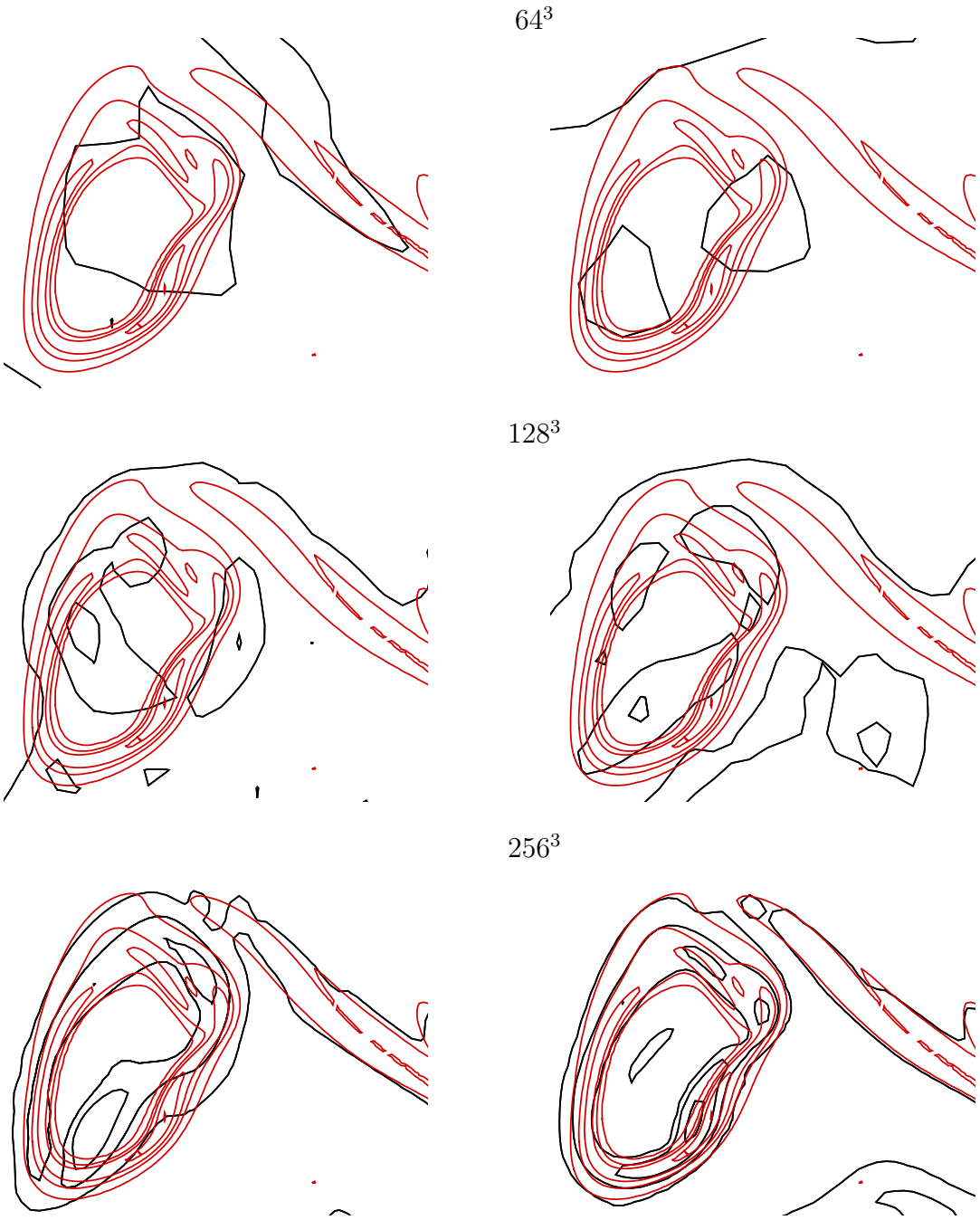

Figure 6: Contour of dimensionless vorticity norm $\frac{L}{U_0}\|\omega\| = 1, 5, 10, 20, 30$ in a subset of the periodic face $\frac{x}{L} = -\pi$ at time $t^* = 8$ on the three grids. Comparison between reference results in [5] (red) and SPARK-LES results (black) for fourth-order (left) and sixth-order (right) compact schemes.

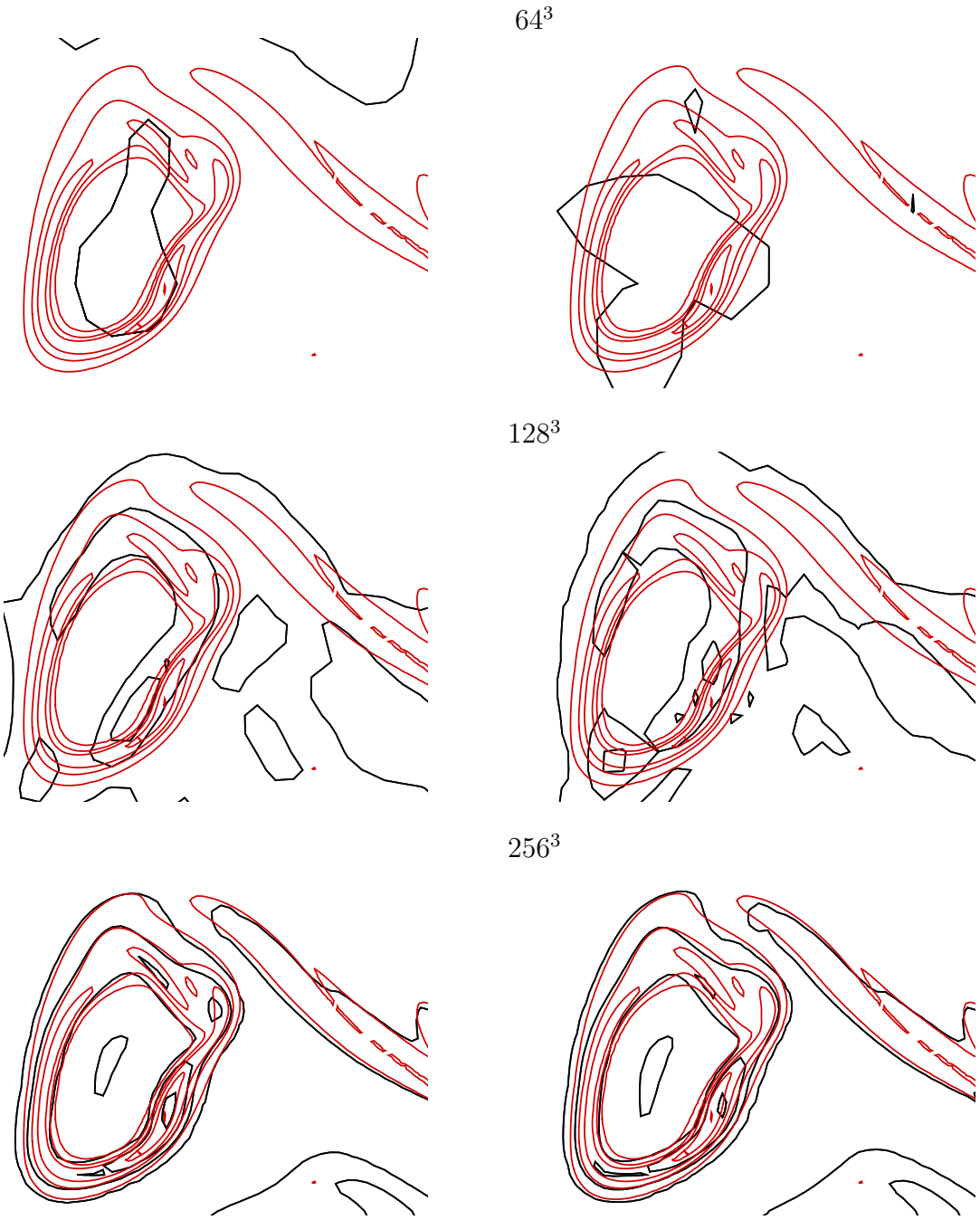

Figure 7: Power spectrum $E^*(k)$ for second-order (left) and fourth-order (right) explicit schemes.

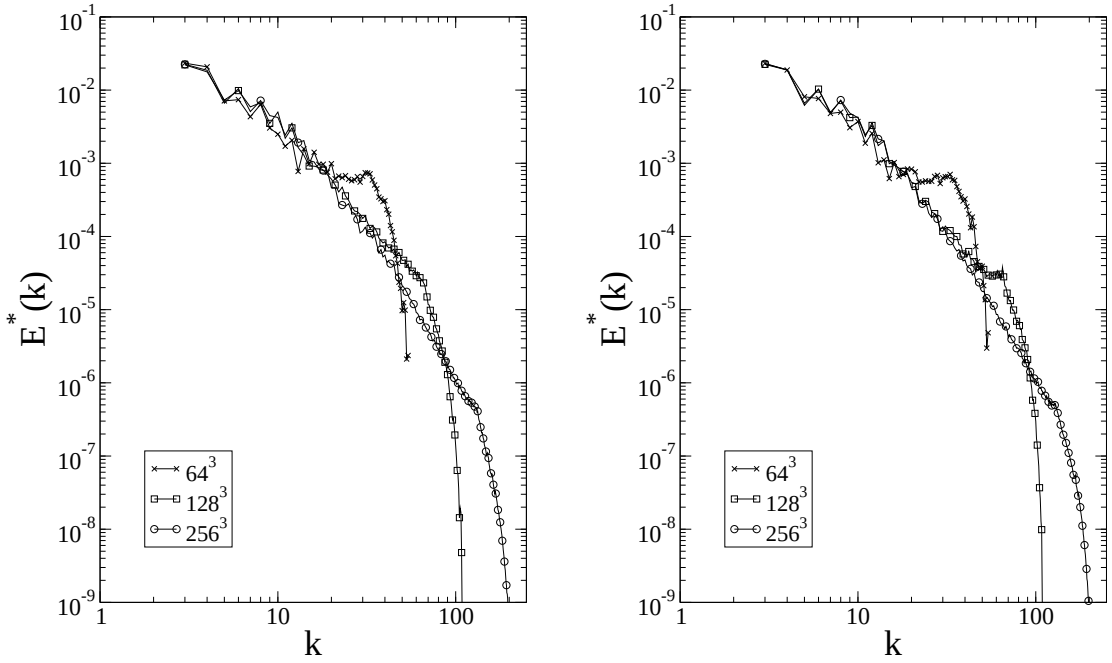

Figure 8: Power spectrum $E^*(k)$ for fourth-order (left) and sixth-order (right) compact schemes.